Journal of Structural Geology 37 (2012) 19–35

Contents lists available at SciVerse ScienceDirect

Journal of Structural Geology

journal homepage: www.elsevier.com/locate/jsg

Architecture and growth of normal fault zones in multilayer systems: A 3D field analysis in the South-Eastern Basin, France

V. Roche [a,b,*], C. Homberg [a], M. Rocher [b]

[a] UPMC, Univ. Paris 06, ISTEP, UMR 7193, 4 place Jussieu 75252 Paris Cedex 05, France
[b] IRSN (Institut de Radioprotection et de Sûreté Nucléaire), PRP-DGE/SEDRAN/BERIS, B.P.17, 92262 Fontenay-aux-Roses Cedex, France

ARTICLE INFO

Article history:
Received 9 January 2012
Accepted 5 February 2012
Available online 14 February 2012

Keywords:
Fault growth
3D fault architecture
Multilayer system
Normal fault zone
Clay sub-horizontal fault
Displacement profile

ABSTRACT

3D field data on mesoscale normal faults were collected to examine the geometries and growth of faults in multilayer systems. Observation and analysis of the fractures include the collection of geometric attributes such as fault dips and fault zone thicknesses, detailed mapping in cross-sections and plan views, and the construction of individual and cumulative displacement profiles. Fault zone growth is consistent with a "coherent model" and is strongly influenced by the multilayer system. In the limestone layers, faults grew in several steps, including opening and frictional sliding on 80° dipping segments. Faulting in clay layers was in the form of 40° dipping faults and sub-horizontal faults, the latter being mostly early features developed under the same extensional regime as normal faults and disturbing the fault architecture. The fault zone thickness increases with the limestone thickness and the presence of sub-horizontal faults in clay beds. Numerous connections occur in clay units. The moderate ($\approx$0.08) and low ($<$0.03) mean displacement gradients in clays and in limestones respectively indicate that the vertical propagation of faults is inhibited in clay layers. Analysis of displacement along fault strike indicates that a 0.08 displacement gradient is associated with the horizontal propagation of fault segments in limestones. According to this value, the fault zones are much longer than expected. It is associated with 'flat topped' displacement profiles along some fault segments and connection between segments to form complex fault zones.

1. Introduction

In anisotropic multilayer systems, fractures are commonly restricted to competent layers like limestones or sandstones (Nicol et al., 1996; Gross et al., 1997; Wilkins and Gross, 2002; Soliva and Benedicto, 2005), but faulting into adjacent clay layers also occurs at various scales, depending on parameters such as the thickness of the clay layer, its rheological properties, and fault displacement. Thus faults can cross-cut a multilayer sedimentary system and often form complex deformation zones referred to as fault zones. Fault zones include several fault segments that may or may not connect (Segall and Pollard, 1980; Peacock and Sanderson, 1991; Cartwright et al., 1995; Childs et al., 1996; Crider and Pollard, 1998; Peacock, 2002; Walsh et al., 2003) and secondary fractures related to the damage zone (McGrath and Davison, 1995; Kim et al., 2004).

The Callovian–Oxfordian indurated clay formation, sandwiched by two limestone units, is currently being studied in Eastern France as a potential site for deep geological disposal of long-lived intermediate and high-level radioactive waste. The safety of such a repository is partly based on the capacity of the clays to retard the propagation of tectonic fractures from the enclosing limestone formations which could act as conduits for the migration of radioactive solutions to the biosphere. Because the resolution of geophysical survey methods (e.g., seismic reflection) is not high enough to identify faults with small throws (e.g., $<$10 m) in clays, faults must be studied in outcrops to characterise their geometries and impact on fluid flow in multilayer systems. Such knowledge and tools could also assist reservoir exploration and improve understanding of strain localization in heterogeneous rocks.

Numerous studies have investigated fault growth and concluded that the heterogeneity of a multilayer sedimentary system partially controls the fault zone characteristics. For instance, fault dips commonly change with lithology (Mandl, 1988; Ferrill and Morris, 2003; Schöpfer et al., 2007) and linkages may occur preferentially within layers or at layer interfaces (Peacock and Zhang, 1993; Childs et al., 1996; Mansfield and Cartwright, 1996). The geometry (fault orientation and segmentation) and kinematics (displacement profiles) of natural fault zones are generally derived from 2D observations, either in cross-sections or in map views. Such studies

* Corresponding author. Fax: +33 (0) 1 58 35 77 27.
E-mail addresses: vincent.roche@irsn.fr, vincroche@hotmail.fr (V. Roche).

0191-8141/$ – see front matter © 2012 Published by Elsevier Ltd.
doi:10.1016/j.jsg.2012.02.005

are essential to understanding the processes that govern fault geometries and growth such as fault interaction and linkage, joint reactivation, fault restriction by lithological barriers, and heterogeneity in the stress field (Segall and Pollard, 1980; Muraoka and Kamata, 1983; Petit and Mattauer, 1995; Wilkins et al., 2001; Soliva and Benedicto, 2005). However, fault growth is a 3D process. Walsh et al. (2003) discussed the bias caused by the 2D nature of most observations and models, and concluded that 2D observations are not conclusive to establish a fault growth model. Some studies focus on this topic using seismic data (Mansfield and Cartwright, 1996; Kattenhorn and Pollard, 2001), analogue and numerical models (Willemse et al., 1996; Marchal et al., 2003) and outcrop observations (Kristensen et al., 2008).

In this paper we present detailed field data from four mesoscale normal fault zones cutting through clay and limestone beds that are several tens of centimetres thick. The faults have a small amount of slip (a few decimetres) and thus provide information about the early stages of fault development. The fault zone architecture and the displacement profiles obtained from these examples are examined with a 3D perspective thanks to the normal bedding and parallel bedding sampling and are used to discuss the parameters governing fault growth in multilayer systems.

2. Geological setting and data acquisition

Two outcrops are studied in the Mesozoic South-Eastern French Basin, near the villages of Charce and Espreaux (in the Drôme and Hautes-Alpes departments, respectively). The outcrops are alternating layers of Hauterivian limestone (mudstone) and clay (52% carbonate) (Fig. 1). The limestone and clay layers are 20–60 cm and 10–80 cm thick, respectively. The layers trend N063°E 63°S in Charce and N166°E 66°E in Espreaux. These sequences dip steeply due to shortening which commenced in the Late Cretaceous (Flandrin, 1966). Differential erosion of the limestone and clay layers has produced a 'staircase' morphology of the exposures, i.e. vertical cross-sections of clay-limestone doublet exposures alternate with exposures of the top of limestone layers (Fig. 1). This morphology makes it possible to continuously sample the fault geometries and displacements, both vertically (Figs. 2, 4 and 6) and parallel to the fault strike (Figs. 3, 5 and 7), therefore giving some degree of access to the 3D geometry of the fault zones.

The outcrops are cut by three mesoscale normal fault zones (one in Charce and two in Espreaux). We refer to these as the Charce fault zone, and the Espreaux A and Espreaux B fault zones. They comprise several, often sub-parallel faults (slip surfaces) whose shear displacement is indicated by the offset of bed boundaries and/or by slip indicators (i.e. slickenside). The faults commonly exhibit many geometrical complexities. In this paper and following Peacock et al. (2000), a fault segment refers to a finite slip surface (with possible inflections) either with isolated tips or with tips that connect to another surface. In the volume adjacent to fault segments, we also recognized small dipping fractures without any visible displacement within clays, named associated fractures. In addition, numerous small-scale normal faults located outside the main fault zones were identified. We also observed sub-horizontal faults in clays (CHF) and strike-slip faults. Bed parallel joints forming several dense sets within limestones were also observed.

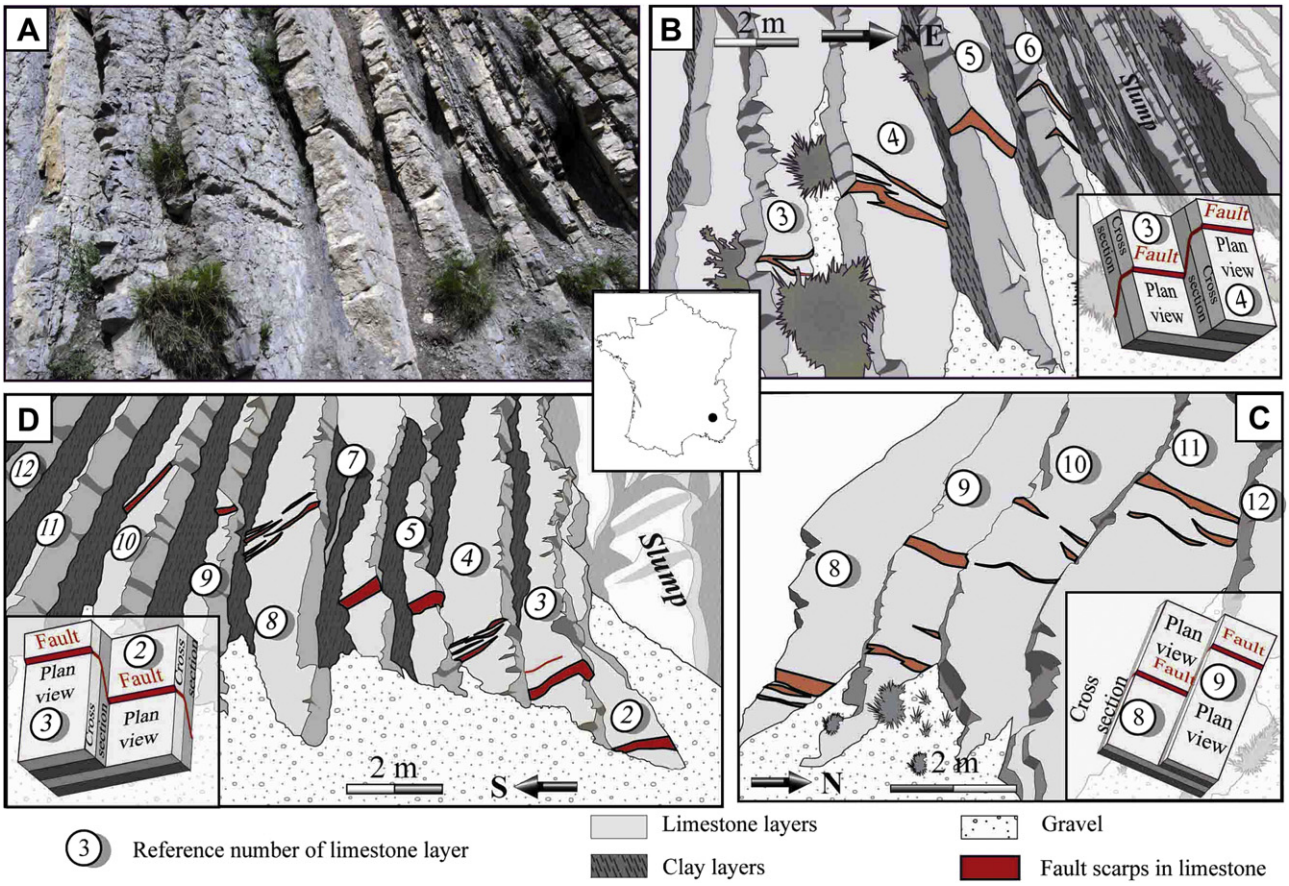

Fig. 1. General view of the three normal fault zones cutting through the Hauterivian clay/limestone multilayer system of the South-Eastern Basin, France. A: Photograph of fault zone A in Espreaux. B, C, and D: Photo-interpretations of fault zone A in Espreaux, fault zone B in Espreaux and fault zone in Charce. Block diagrams show how the fault zones are successively exposed in clay-limestone doublet cross-sections and on the top of the limestone beds (plan view). Numbers refer to limestone layers.

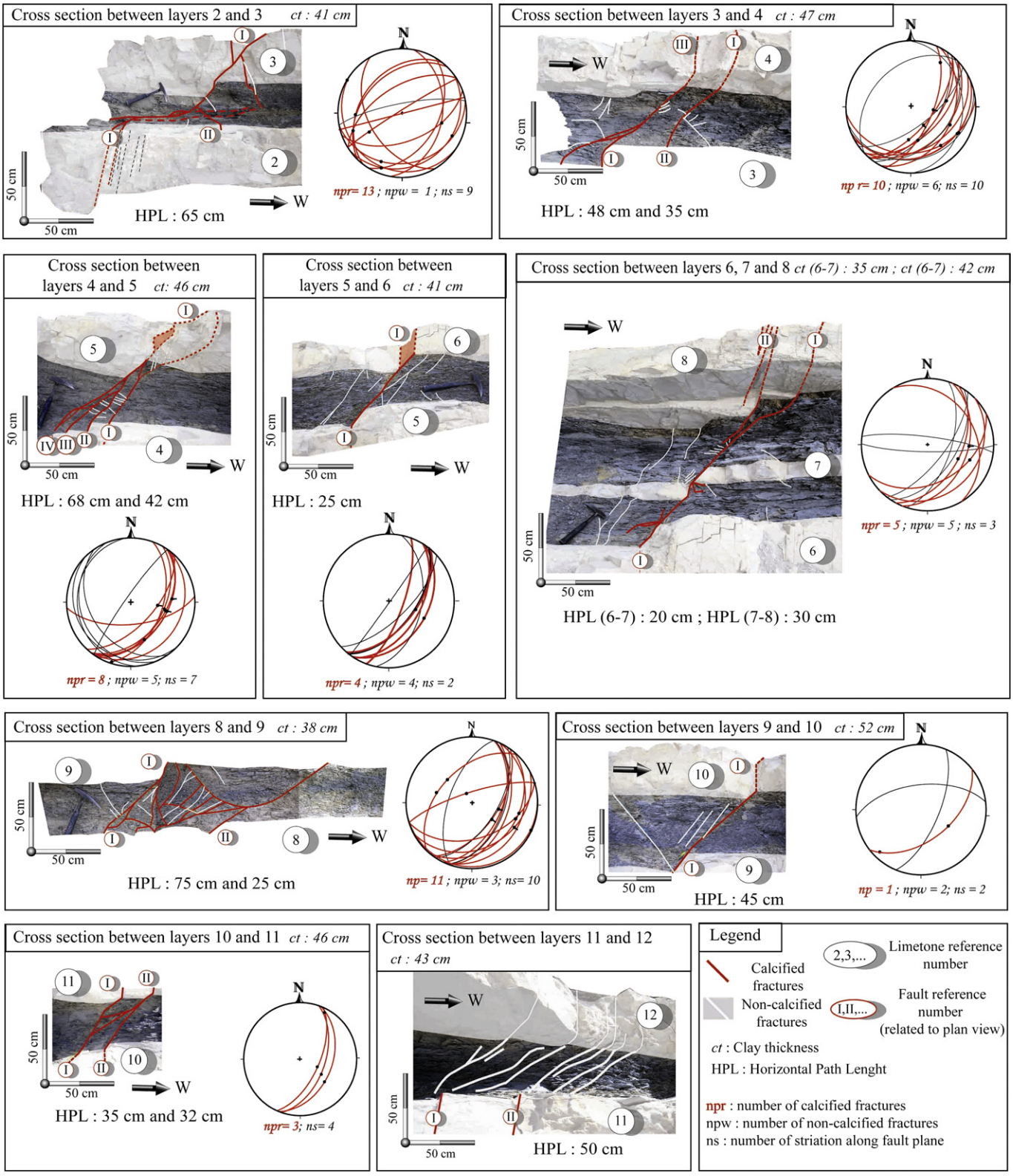

Fig. 2. Back-titled cross-section data of the Charce fault zone. Fractures associated with the fault zone are mapped in each clay-limestone doublet cross-section. Their orientations are shown in stereographic projection (equal-area, lower hemisphere): fracture planes as solid great circles and slip vectors for faults as dots. The fault zone path length (see main text) and the clay thicknesses are indicated. See Fig. 1 for limestone reference numbers.

Observations and measurements of the outcrops include (1) detailed mapping as well as systematic measurement [i.e. strikes, dips and slip vectors (where visible)] of the fault segments and other fractures along the vertical cross-sections (CS) and along the top of the limestone units (referred to as plan views, PV); (2) collection of displacement data on each fault segment; (3) collection of data describing the spatial arrangement of the faults zones, i.e. horizontal path length (HPL) or the fault zone thickness (FT) (see

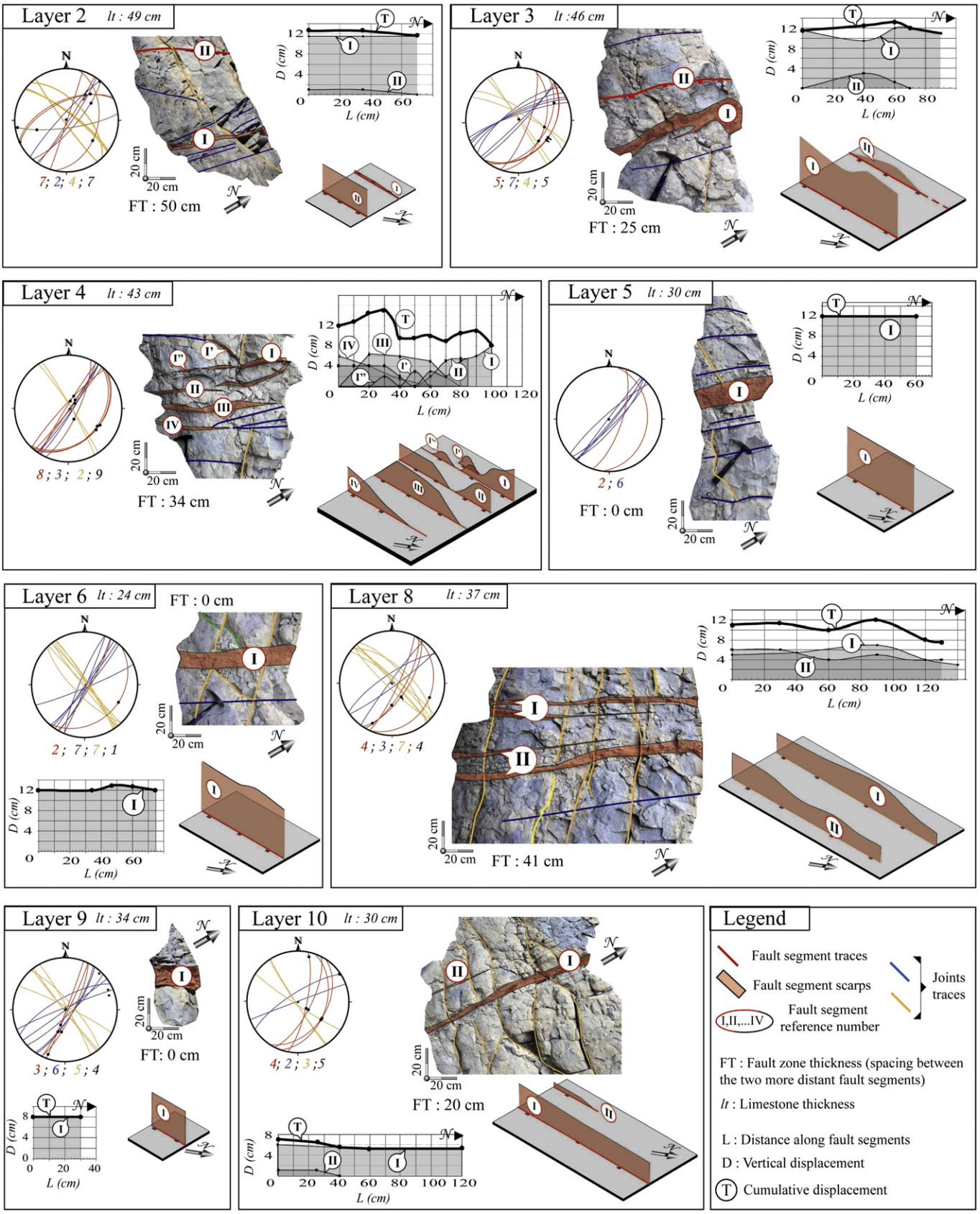

Fig. 3. Back-tilted plan view data of the Charce fault zone. Fractures associated with the fault zone are mapped on the top of each limestone unit, as well as secondary fractures. Their orientations are shown in stereographic projection (amount for each data type indicated). Graphs illustrate the displacement profiles on each fault segment (thin lines) also shown in a 3D perspective representation, as well as the calculated cumulative displacement (thick line). Reference numbers of faults and limestone layers are the same as in Fig. 2. The fault zone thickness (see main text) and the limestone thickness are indicated. Same legend as in Fig. 2.

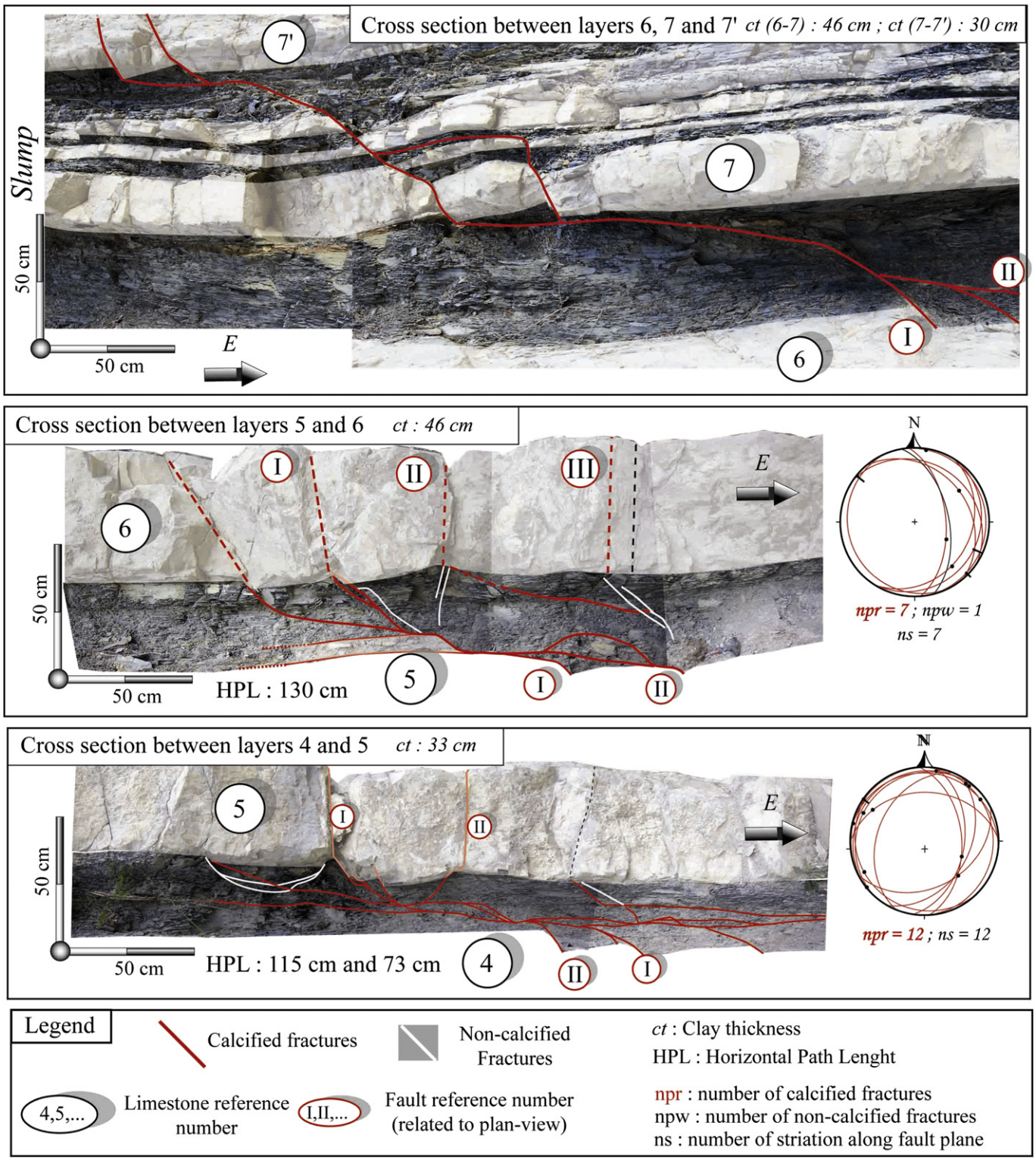

Fig. 4. Back-titled cross-section data of the Espreaux A fault zone. Same legend as in Fig. 2.

section 4), and (4) measurement of clay and limestone layer thicknesses. Along each fault zone, the trace of the faults and fractures was mapped on scaled CS (Figs. 2, 4 and 6) and PV photographs (Figs. 3, 5 and 7). Fault zone data are also presented in stereographic projections (Fig. 8) in which we distinguish data from clays and data from limestones. Data on joints, strike-slips and CHFs are plotted in separate stereonets diagrams. We also undertook a statistical analysis of the joint set spacing using both PV and CS observations.

For each fault segment, the separations on limestone bed boundaries were measured normal to the bed. These measurements are considered to be equivalent to fault throw at the time of faulting and prior to bed tilting (see below). The fault throws were sampled in PV, along the fault segment traces. These data were

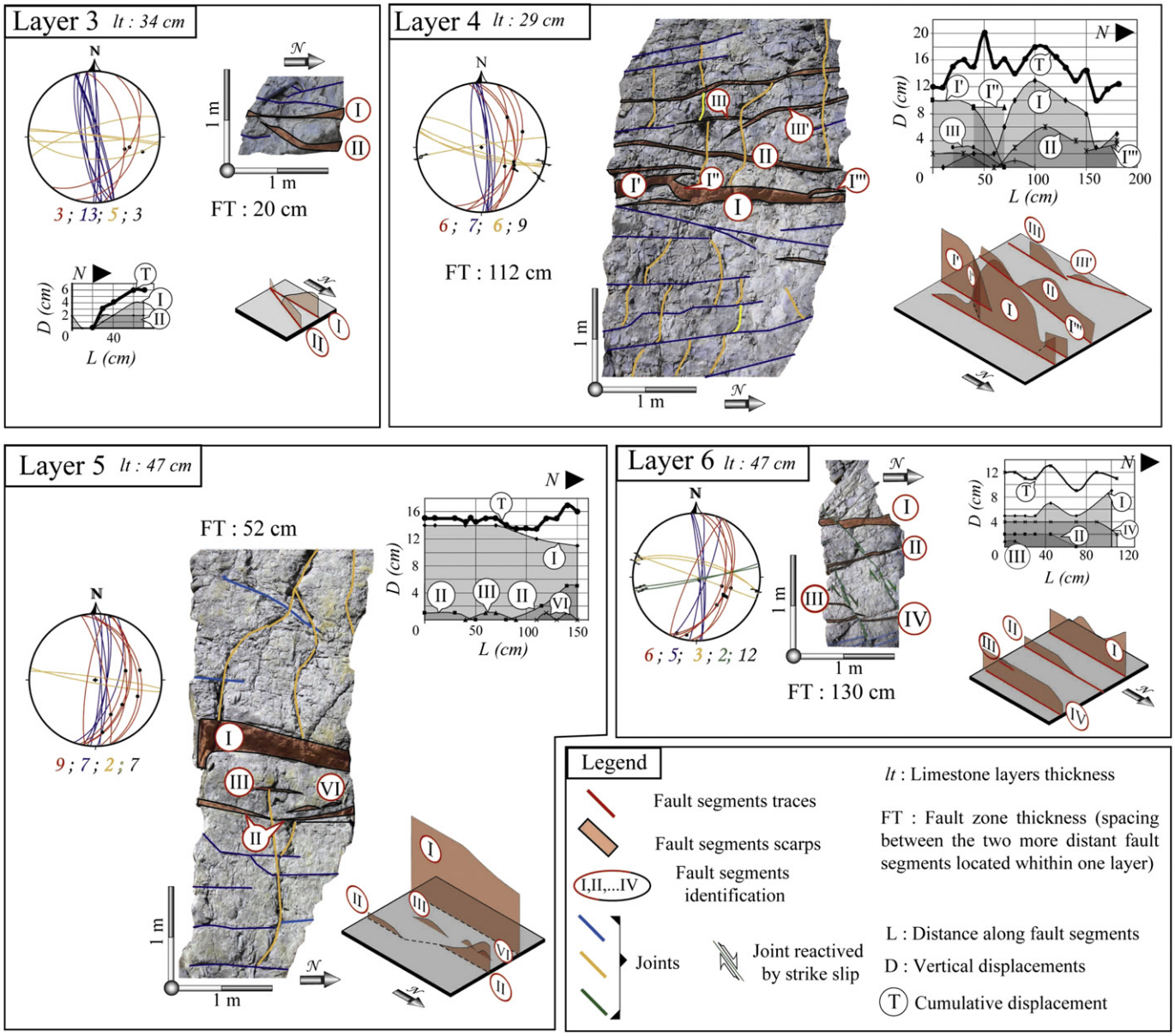

Fig. 5. Back-tilted plan view data of the Espreaux A fault zone. Same legend as in Fig. 3. Reference numbers of faults and limestones are the same as in Fig. 4.

used to construct bed-normal and strike-parallel displacement profiles for each fault segment (Figs. 3, 5 and 7) which were used to discuss the vertical and horizontal components of fault propagation. We also calculated the cumulative CS and PV displacement profiles for the fault zone by summing the throws of each individual fault segment. By adding end to end the CS and PV cumulative displacement profiles, we show in Fig. 12 how the cumulative displacement varies vertically and laterally along each fault zone. Given that the observations were made by the naked eye and measurements were made using a ruler, the throw uncertainty is close to ±0.5 cm.

When observed after having removed the bed tilting, the fault segments exhibit refractions as a function of lithology (Figs. 2, 4 and 6) similar to those typically observed along normal faults cutting multilayer systems. Because these fault zones are now identified in strongly dipping strata, we calculated their original attitude by restoring bedding to the horizontal. The state of stress under which the segments and the additional normal faults slipped was also calculated using the software of Angelier (1990). This method is based upon the hypothesis that faults slip in the direction of the resolved shear traction (Wallace, 1951; Bott, 1959). This assumption allows the orientations of the three principal stresses, σ_1, σ_2 and σ_3 to be estimated ($\sigma_1 > \sigma_2 > \sigma_3$, compression positive). In Espreaux, both studied fault zones are located on the eastern limb of a ~N–S anticline and additional normal faults also cut the western limb (not shown in the figures). Thus for this site the stress inversion across the fold provides a conclusive test for the age of faulting relative to folding (compare H and J, Fig. 8). After back-tilting, the faults exhibit typical normal fault set attributes (i.e. high dips, dip slips both on synthetic faults and the few conjugate faults) and the calculated maximum principal stress (σ_1) is nearly vertical (Fig. 8J), indicating that fault slipped before bed tilting. The same conclusion is reached for the Charce fault zone (Fig. 8G,I), although the fold test is less constrained in this case because fault data were collected from a single fold limb.

The absolute age of faulting cannot be determined from our data. The directions of minimum principal stress (σ_3) trend N106°E and N129°E in Charce and Espreaux, respectively (Fig. 8I,J). The similarity may indicate that the normal fault zones result from the

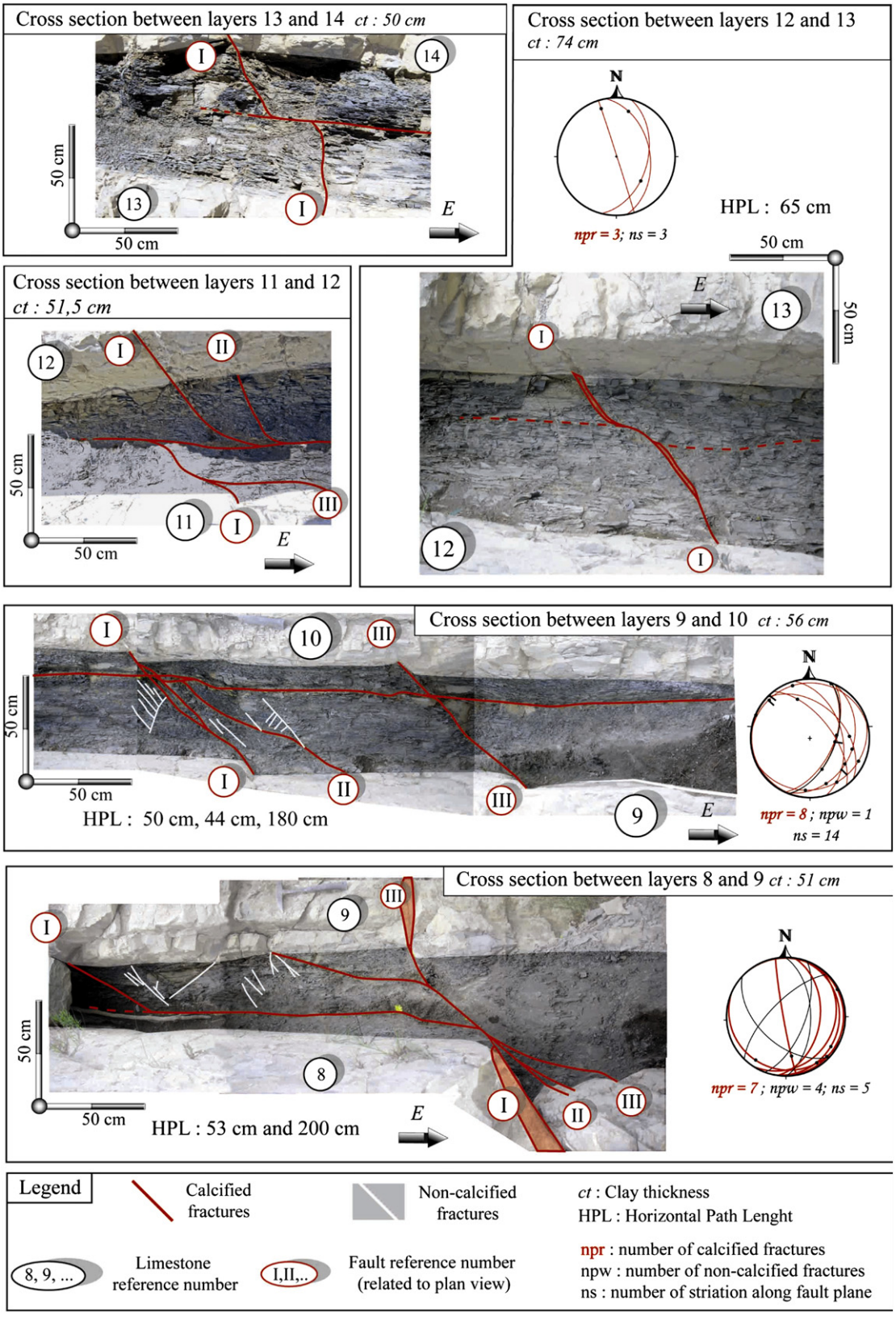

Fig. 6. Back-titled cross-section data of the Espreaux B fault zone. Same legend as in Fig. 2.

same tectonic event. This orientation is close to that associated with the Oligocene rifting, which affected the European platform before the Late Mesozoic to Cenozoic inversion and its associated folding (e.g., Bergerat, 1987). The normal faults studied may have formed before the Oligocene, but whatever their exact age they are not synsedimentary because they affect slumps. The chronology of the other fractures will be discussed in the next section on the basis of geometrical relations. Because all fractures formed before tilting,

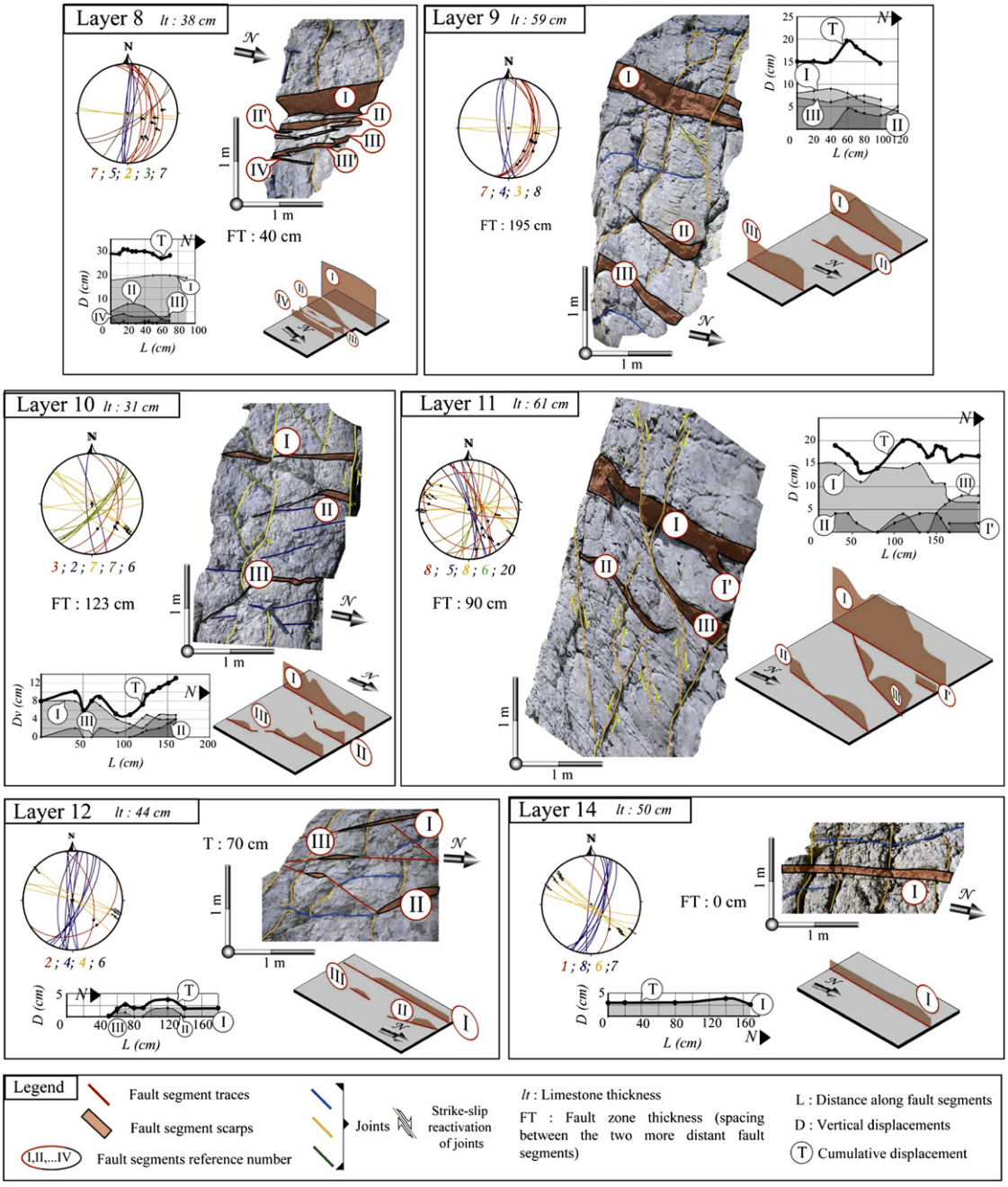

Fig. 7. Back-tilted plan view data of the Espreaux B fault zone. Same legend as in Fig. 3. Reference numbers of faults and limestones are the same as in Fig. 6.

they are presented in the next sections and in the figures after restoration of their original attitudes and thus after back-tilting. We also include data from a fourth normal fault zone outcropping near Rosans (Hautes-Alpes). This fault zone affects the same Hauterivian sequence and the maximum offset is close to 3 cm. The detailed geometry of this normal fault will not be presented in detail.

3. Fracture types and fracture orientations within the multilayer systems

3.1. Normal fault zones

The Charce, Espreaux A and Espreaux B fault zones have maximum throws of 15 cm, 20 cm, and 31 cm, respectively. Strike-parallel and bed-normal outcropping lengths range from 5.1 m to 6.7 m and from 3.4 m to 4.8 m. Each fault zone comprises several sub-parallel fault segments filled with calcite, which is usually very thick in the limestone layers and thinner in the clay layers. Fault surface striations are generally well preserved in limestone units and are sometimes visible in clays. Except near linkage areas the fault segments have a near-constant strike, N035°E and N010°E on average in Charce and Espreaux, respectively (Fig. 8A,B). By contrast, large dip variations are observed. In the limestone units, the dip distribution of the normal faults exhibits two major peaks (Fig. 9A): the first equals 80°, a value close to that of joints (see below); the second ranges between 30° and 50° and corresponds to the fault attitude at the clay/limestone contact (Figs. 2, 4 and 6). In the clay layers, fault segments have much lower dips than in the limestone layers with mean values of 30°–50° (Fig. 9C). Thus the three fault zones studied exhibit high refraction as a function of the lithology.

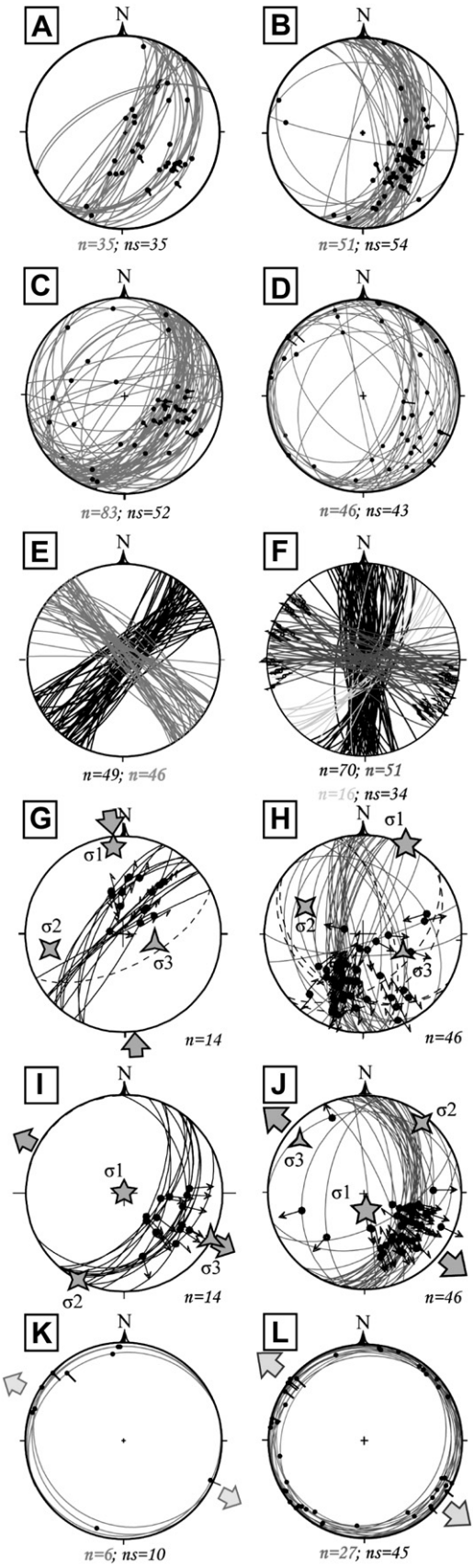

Fig. 8. Stereographic projection of the Charce (A, C, E, G, I and K, right column) and Espreaux (B, D, F, H, J and L, left column) fractures. A and B: normal fault zone segments in limestones. C and D: fractures in clay layers. E and F: joints (black, light and very light grey for the various sets) and strike-slip faults in limestones. G, H, I and J: calculated stress state using faults in their present-day (G and H) and back-tilted attitudes (I and J). Data includes segments of the main fault zone as well as additional normal faults (striae without clear direction excluded). K and L: sub-horizontal fault in clays (CHF). All data, except in G and H, are shown in their back-tilted attitudes (lower hemisphere, equal area projection). Note that the trend of several striae in CHFs is similar to the minimal principal stress inferred from inversion of fault slip data. Fault planes are solid great circles and bedding is the dashed great circle. Slickenside lineations are dots with small lines or small arrows (divergent, convergent, and double for normal reverse, and strike-slip motion respectively) when direction of movement was determined. The calculated maximum (σ_1), intermediate (σ_2), and minimum (σ_3) stresses are stars with 5, 4, and 3 branches. Convergent and divergent grey arrows point in the direction of the calculated compression and extension in G, H, I and J; the directions of extension calculated in I and J are also reported in K and L respectively. n indicates the amount of data and ns stands for the number of striae.

The associated fractures observed within clays and very close to fault segments are non-calcified and may be locally numerous, especially close to fault segment connections. They display no visible evidence of displacement and are quite variable in orientation. Some of them are sub-parallel or sub-conjugate to the fault segments; others strike-parallel to joints. These variations may indicate complex local movements related to local accommodation.

3.2. Sub-horizontal faults in clays

In both outcrops we identify faults that are almost parallel to bedding and located within some of the clay layers. They are referred to here as clay sub-horizontal faults (CHFs). CHFs have dip values within about 10° of the dip of the bed and are filled by thin calcite. Although accurate determination is difficult for such low dipping planes, data suggests a degree of variation in the fault strike (Fig. 8K,L). CHFs extend outside of the normal fault zones in most cases. CHFs are also observed within clay layers that are not affected by the normal fault zones (i.e. the upper or lower layers in the exposed sequence). The CHFs may abut fault segments and sometimes seem to be offset by the fault segments by a few centimetres (CS 6–5 in Fig. 4, CS 8–9 and CS 12–13 in Fig. 6). The opposing configuration is also observed (for example CS 4–5 in Fig. 4, fault I in CS 8–9, fault II in CS 9–10 and CS 13–14 in Fig. 6). In other cases the fault segments and the CHFs cross-cut without offset (for example CS 4–5 in Fig. 4, fault I and III in CS 9–10 in Fig. 6). These contrasting chronological relationships may suggest that the CHFs slid at the same time as the fault segments. In some cases their presence outside of the fault zones is difficult to constrain (CS 2–3 in Fig. 2 or CS 12–13 in Fig. 6).

Two similar striation sets are identified on the CHFs. One of them exhibits a horizontal component of the movement of the top of the clay units in the same direction as that of the hanging wall of the fault zones. The mean direction of these striae is similar to the N106° and N129° orientation of the σ_3 inferred from inversion of slip data from the normal fault zones (Fig. 8K,L). These observations suggest a kinematic relationship between the normal fault zones and CHFs. The CHFs also bear a second set of striae but without any visible sense of movement and trend N–S and NE–SW in Charce and Espreaux, respectively. These slip directions are similar to those of the compressions suggested by strike-slip faulting and by stylolized planes. Whatever the age of this second movement, it may have altered the fault zone architecture (CS 11–12 in Fig. 6), but not significantly because in most cases no large offset of the normal fault segments has been observed.

3.3. Other fractures and relative chronology

The limestone beds are cut by other short fractures not related to the normal displacement on the main fault zones described

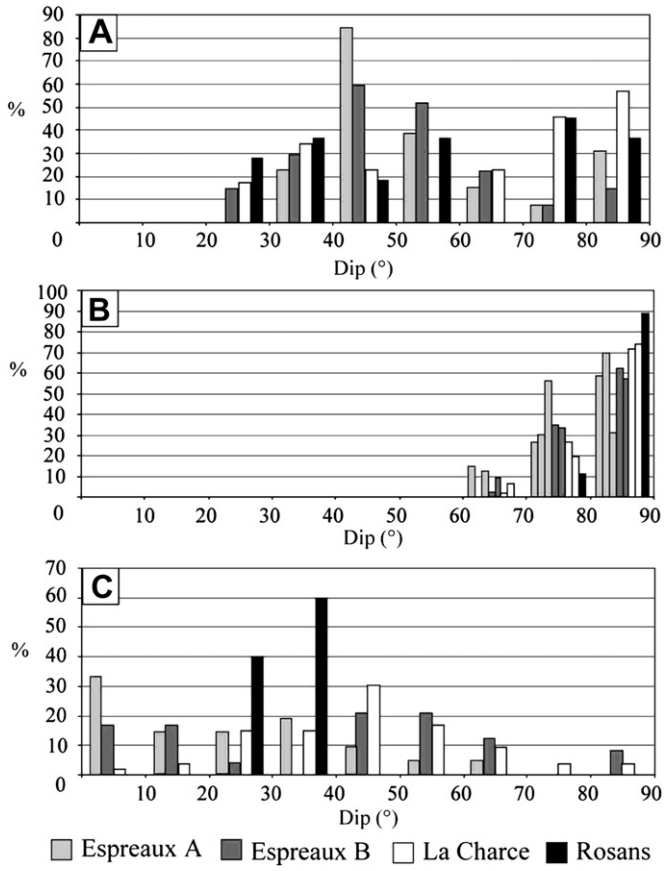

Fig. 9. Frequency histogram of back-tilted dip data. Data from the Espreaux, Charce and Rosans fault zones. A: Fault segments in limestones. B: Joints (all joint sets included) in limestones. C: Fault segments in clays. Faults not associated with the normal fault zones are excluded here.

above. The most numerous fractures are joints, without calcite mineralization. These joints are almost perpendicular to bedding, suggesting that they formed before bed tilting. On the basis of their strikes before tilting, two joint sets trending NE–SW and NW–SE were identified in Charce (Fig. 8E) and three sets, trending N–S, WNW–ESE and NW–SE, were recognized in Espreaux (Fig. 8F). Thus the Charce NE–SW and Espreaux N–S sets are almost parallel to the fault zones. Other fractures cutting the limestone layers are small-scale normal faults in both areas, strike-slip faults in Espreaux, and stylolized planes in Charce. Given their attitudes, all these features predate tilting. The small-scale normal faults, with offsets below several centimetres, exhibit similar orientations to those of the main fault zones. Sinistral strike-slip faults trend between NW–SE and E–W in Espreaux and a few ENE–WSW dextral faults were also observed (Fig. 8F). No fault slip inversion was performed on them but their orientations suggest that they formed under E–W compression, a direction similar to the shortening that produced folding at this site. The ENE–WSW stylolite teeth in Charce probably result from the same event.

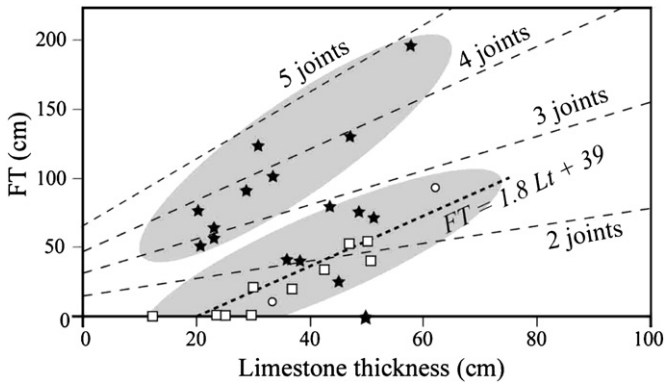

Fig. 10. Fault zone thickness (FT) versus limestone thickness. Data from the Espreaux, Charce and Rosans fault zones. The fault zone thickness is the distance measured bed parallel and normal to fault strike, between the most distant fault segments in one limestone unit. Symbols refer to the presence (black star) or absence (open square) of sub-horizontal faults (CHFs) in the surrounding clay units. Open circles are undefined data. Dashed-lines are the theoretical distances between a joint and its second (3 joints), third (four joints) and fourth (5 joints) nearest neighbours obtained from a statistical analysis of the three exposures studied. Grey shading delimits a subdivision into two groups. See main text for further explanations.

As discussed above, the small-scale faults, the joints, and the stylolites predate folding. The strike-slip faults may offset the segments of the normal fault zones but not by more than a few centimetres (example Fig. 5 layer 6 or Fig. 7 layer 11). These late movements therefore do not alter the overall geometry of the normal fault zones. Moreover, when the fault segments show strike-slip reactivation, the slip occurred in the horizontal direction so that the original throw along the normal fault segment was preserved. No cross-cutting relation was observed between the joints and the mesoscale normal faults. Joints are commonly reactivated or offset by the strike-slip faults and are sometimes stylolitized. Thus the joints are interpreted to predate the compression events. Moreover, the joints do not show significant modification in orientation when approaching the normal fault zones (Figs. 3, 5 and 7). Because stress directions are generally deflected close to fault zones (Petit and Mattauer, 1995; Kattenhorn et al., 2000; Homberg et al., 2004), this suggests that the joints predate faulting, which is often the case in a sequence of brittle deformation (Hancock, 1985).

4. Fault zone spatial arrangement

4.1. Fault splays and fault connections

The number of the fault segments varies along the fault zones and the sedimentary multilayer system (Figs. 2–7 and see also Fig. 14 for a synthetic view). Observations on CS indicate that no fault segments abut layer boundaries, including those with displacements of less than 1 cm (Figs. 2, 4 and 6). Close to layer boundaries, the number of fault segments is therefore comparable in clay layers and the adjacent limestone layers. The number of segments may however decrease considerably through the clay layer because several connections occur in CS due to the difference in dip from one fault to another (see for example CS 3–4, 4–5 in Fig. 2; CS 6–7′ in Fig. 4). These connections observed on CS present the following characteristics: (i) the fault segment with small displacement predominantly connects on the major fault segment (see for example connection on fault IV in CS 4–5 in Fig. 2 and connection on fault I in CS 5–6 in Fig. 4); (ii) connections occur both in the hanging-wall and in the foot-wall of the major fault segment; (iii) connections occur mainly between closely spaced fault segments. The fault segments may also branch on the CHFs so that the fault zone is locally composed of a single CHF (see for examples CS 4–5 in Fig. 4).

Fault connections were also observed in PV on the top of limestone layers (see for example the connections between fault segments I, I′ and I″ in layer 4 of Fig. 5 and the connection between I and I′ in layer 11 in Fig. 7). These connections occur through changes in the fault orientation at the very end of one or of both fault segments. In these cases, the two fault segments generally show a decrease in displacement when approaching one another and the cumulative displacement may show a local variation in the

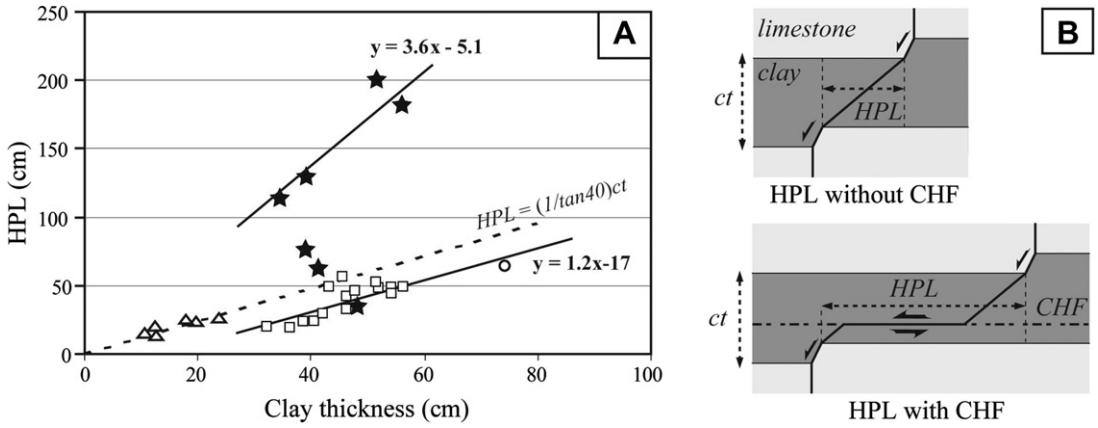

Fig. 11. A: Horizontal path length (HPL) in clay units versus clay thickness. The horizontal path length is the horizontal distance (measured bed parallel and normal to the fault strike) separating the fault segments in the upper and lower limestones (see right-hand diagram). Solid lines are regression lines. Black stars and open squares refer to the presence and absence of sub-horizontal faults (CHF) in the Charce and Espreaux fault zones. Measurements from Rosan are open triangles (no CHFs). The dashed line is the theoretical horizontal path length for a 40° dipping fault in a clay unit. The Rosans data fits this dashed line. The Espreaux and Charce regression lines (thin line) for data without CHFs have the same slope as the dashed line.

overlap zone. These geometric and kinematic attributes are characteristic of relay zones (Peacock and Sanderson, 1991; Cartwright et al., 1995; Crider and Pollard, 1998). Such connections may occur in clay layers but could not be observed because no PVs of these units are exposed.

4.2. Fault zone thickness

As described above, the fault zones include one or more sub-parallel and close spaced fault segments in limestone layers. The fault segments sometimes overlap along a significant horizontal distance and may connect with each other. The fault zone within limestone layers may therefore vary in PV. Its maximum value, measured bed parallel and normal to fault strike, is referred to here as the fault zone thickness (FT). The fault zone thickness is plotted against the thickness of the limestone layers for the four fault zones studied and with various symbols according to the presence of CHFs (Fig. 10). In each limestone layer, we also carried out a statistical analysis of joint spacing, i.e. normal distance between two joints of the same set (299 spacing measurements on 23 limestone layers). Whatever the outcrop or the joint set, the average spacing of joints is constant in each layer and is directly proportional to the limestone layer thickness (i.e. joint spacing is close to limestone thickness). This joint-normal distance is plotted as a function of limestone thickness in Fig. 10 ("2 joints" line). We also calculated the distance between a joint and its second ("3 joints"), third ("four joints") and fourth ("5 joints") nearest neighbours in the array as a function of limestone thickness and plotted the corresponding straight lines in Fig. 10.

Fault zone thicknesses range from 0 to 2 m. If no CHF occurs in both the underlying and overlying clay layers, the fault zone thickness increases with the thickness of limestone layer. The fault zone thicknesses are much more scattered when CHFs occur, but it seems that they follow two tendencies. A first group is close to the population without the CHFs and a second group is characterized by much higher values of fault zone thickness. For the latter, the fault zone thickness also increases with the thickness of the limestone layer. These observations indicate that the fault zone thickness depends on the limestone thickness and may increase considerably where CHFs are present in the neighbouring clay units.

The fault zone thicknesses are not comparable to the theoretical spacing between two or more joints, suggesting that the joint spacing do not strongly influence fault zone thickness in the cases studied. This observation may be consistent with the joints post-dating faulting, but accepting that joints predate fault zones (see sub-section 3.3), although some fault segments may have reactivated joints, this was generally not the case. It is particularly obvious far away from the clay units with CHFs, where some fault zone thicknesses are smaller than the spacing between two joints and where the fault zone includes several sub-parallel segments, which are inferred to have developed between the joints.

As discussed before (see sub-section 4.1), the number of fault segments close to the bed boundaries is the same within limestones and clays. However, due to the lower dips of fault segments as well as to their connections to the CHFs, the fault zone is generally thicker in the clay layers (see CS 2–3 in Fig. 2). It will be recalled that the fault zone thickness refers here to the bed parallel thickness of the faulted host rock. This definition is appropriate for purposes that entail estimating the maximum lateral extent of faulted clays associated with the faults in neighbouring competent layers. For other purposes, it would be more relevant to examine the fault thickness in a direction perpendicular to the mean fault plane. Due to the numerous fault segment connections in clay units, that value is generally smaller in the centre of the clay layers than in limestones. However, in some places, associated fractures may be very numerous in clay layers and so locally increase the fault zone thickness.

4.3. Fault horizontal path length in clays

Here, we analyse the geometries of fault segments through clay layers by measuring the bed parallel distance between the portions of the fault segment below and above limestones in each clay unit (distance measured bed parallel and normal to the fault strike) (Fig. 11). This distance also represents the length of the bed parallel projection of the fault in clays and is referred to here as the horizontal path length (HPL). The HPL is plotted against the clay layer thickness in Fig. 11, with various symbols depending on whether CHFs are present or not.

Fig. 11A shows that in the absence of CHFs, the HPL is proportional to the clay thickness. Data from Espreaux and Charce fit a straight line that forms the theoretical line characterizing HPL for faults with a 40° dip ($HPL = ct/tan\ 40°$, ct: clay thickness). Because this dip value is close to that measured on the fault segments in the clay layers (Fig. 9), the HPL is directly correlated with the fault dip in

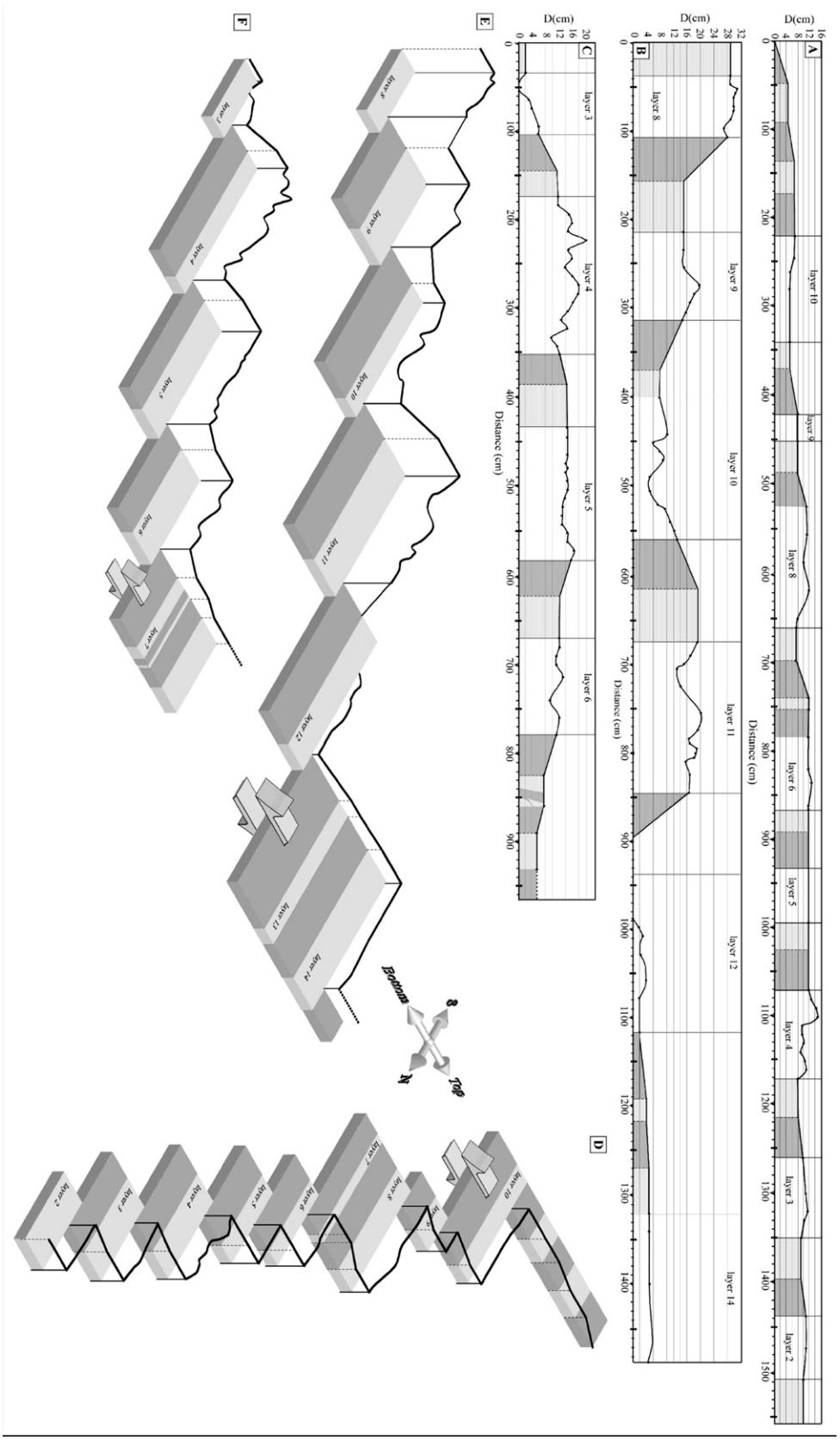

Fig. 12. Cumulative displacement profiles for the three fault zones under study reconstructed by the 'staircase morphology' and showing how the cumulative displacement varies along each fault zone moving first bed-normal (CS), then strike-parallel (PV), then bed-normal again (CS), and so on. A. Charce fault zone. B. Espreaux B fault zone. C. Espreaux A fault zone. CS portions of the cumulative displacement profiles are represented in grey within clay layers and in light grey within limestones layers. PV portions of the cumulative displacement profiles sampled from the top of the limestone are represented in white. The cumulative displacement profiles are also represented in 3D perspective in D, E and F respectively for the Charce fault zone, Espreaux B fault zone and Espreaux A fault zone. Numbers refer to limestone beds. Displacement data is the vertical cumulative displacement over the fault zone and was measured at the top of each limestone unit and on cross-sections exposing clay-limestone doublets.

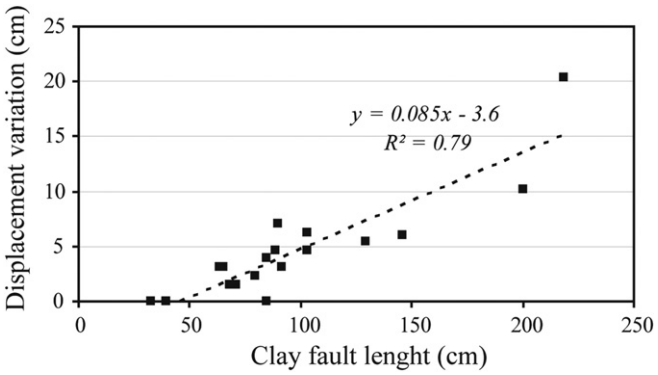

Fig. 13. Displacement variations between limestone units as a function of fault length in clay units.

the clay layer, whatever the clay thickness. The fact that Charce and Espreaux data plot slightly below the 40° clay dip theoretical line arises from a bias in our measurements. Because the HPL was measured from the base of the upper limestone unit to the top of the lower limestone unit (Fig. 11B), this distance decreases slightly with displacement on the upper segment. Therefore, the HPL for the Rosans fault zones, for which the offset is no greater than 3 cm, fits the theoretical line perfectly, whereas the data collected on the Espreaux and Charce fault zones, with displacement of up to 31 cm, is slightly smaller than expected (Fig. 12). For the fault segments connected to the CHFs, the HPLs show far greater values, largely above the 40° clay dip theoretical line, and may reach 2 m (Fig. 11A). The HPLs also seem to increase with the clay thickness and in a much more pronounced manner than in the absence of CHFs. This relation is restricted by limited data, but if true, it suggests that one or more processes control the horizontal path length in this case.

5. Individual and cumulative fault displacement profiles

5.1. Displacement variations along fault segments

Strike-parallel displacement profiles have been constructed along each individual fault segment using measurements from the top of limestone layers. The maximum displacement varies significantly from one fault segment to another, with values ranging from 1 to 20 cm on all fault zones. The profiles exhibit either a flat-topped shape or a more or less elliptic envelope. The elliptic envelope has a maximum value close to the centre of the fault segment, diminishing more or less steadily towards the fault segment tips (see for example: fault segment II, layer 3 or fault segment I″, layer 4 in Fig. 3; fault segment III, layer 5 in Fig. 5; fault segment III, layer 12 in Fig. 7). The two fault segment tips were observed in some cases with fault lengths between 10 cm and 80 cm. For these faults maximum displacement increases with the fault length and the mean displacement/length ratio is 0.045. Observations of fault traces and measurements of displacements indicate that the segments can be longer than the distance of observation and thus longer than 180 cm. The contribution of each fault segment to the cumulative displacement varies along the fault zones and does not show any strong relation with the thickness of the limestone layers, but it seems to depend on the ratio between limestone thickness and surrounding clay thickness. In thick limestone units surrounded by thin clays, fault zones include several faults and cumulative displacement is mainly accumulated by one of them (see layer 5, Fig. 5 and layer 11, Fig. 7). In thin limestone units underlain and/or overlain by thick clays, a single fault segment accommodates the displacement (see layers 5 and 6 Fig. 3). Where the two units have similar thicknesses, the cumulative displacement is distributed over several faults (see layer 8, Fig. 3; layer 4, Fig. 5; layer 9, Fig. 7). The displacement profiles of the fault segments may exhibit complexities such as a steep decline in displacement towards the fault segment tips near a strike-parallel linkage (see for example fault segments I or II in layer 4 in Fig. 3; fault segments I or I′ in layer 4 in Fig. 5; fault segments III in layer 11 in Fig. 7) or an increase or decrease in local displacement in the centre portion of the fault segment (see for example fault segments I in layer 3 in Fig. 3; fault segments I in layer 6 in Fig. 5; fault segments I in layer 10 in Fig. 7). These displacement variations suggest strike-parallel displacement gradients, which range from 0 to 0.7. The values of displacement gradients lower than 0.06 characterize the flat-topped portion of the displacement profiles and the greatest part (60%) of the cumulated length (4200 cm) of all the studied fault segments. Moderate gradients are observed near segment tips (30% of the cumulated length) and equal 0.08 on average. This value is close to the half of the Dmax/L ratio of the fault segments showing two tips (see above). Values larger than 0.18 represent local high displacement gradients (10% of the cumulated length), and are mainly observed near relay zones in PV and are thus likely to reflect the fault segment linkage. Fault segments in clay units are likely to show along-strike variation in displacement but this could not be observed because the top of the clay units is never exposed.

On CS, unfortunately, no reliable internal markers could be identified within the clay units or within the limestone units and thus provide no evidence for displacement gradients within beds. Within limestone units, no variation was observed in CS along fault segments. Given the accuracy of the measurement, CS gradients are thus lower than 0.03 in limestones. There is one exception in limestone layer 4 in CS 3–4 where the displacement decreases from 8 cm to 0 cm in fault segment I (Fig. 2). An opposite variation occurs on fault segment III, suggesting these local variations result from interaction between the fault segments. Thus, these variations are not indicative of the vertical fault propagation. The numerous connections in the clay units preclude us from closely constraining how displacements vary along fault segment in these units, but in a few cases where no connections occur, the displacement gradients are close to 0.09. Note that displacement variations are analysed in the bed-normal direction (and thus along the vertical) in CS rather than along the dip direction of the fault zone. This procedure was adopted because the studied fault zones exhibit frequent connections and fault dip changes. Along straight and sub-vertical fault segments and thus in limestones, the associated gradients are equivalent to those obtained when examining how along-dip displacements vary along the fault dip, as is usually the case in the literature. When the fault path is complex as it is in clay layers, the CS profiles may overestimate the fault gradients and dip analysis of displacement is therefore provided in Fig. 13.

5.2. Strike-parallel and bed-normal cumulative displacement variation

Displacement profiles have been constructed by adding end to end the CS and PV cumulative displacements along the staircase morphology of the outcrops (Fig. 12). For the three fault zones, the cumulative displacement varies significantly through the multilayer system. In the Charce fault zone, the cumulative displacement is rather constant from layer 2 to layer 7, with a small amounts of variation—increase or decrease in PV and decrease in CS—except in layer 4 where there is significant noise along the profile (Fig. 12A,D). Displacement reaches a maximum of 15 cm in layer 4. From layer 7 up to layer 12, displacement almost systematically decreases in CS upward to a zero value in layer 13 but is almost constant or

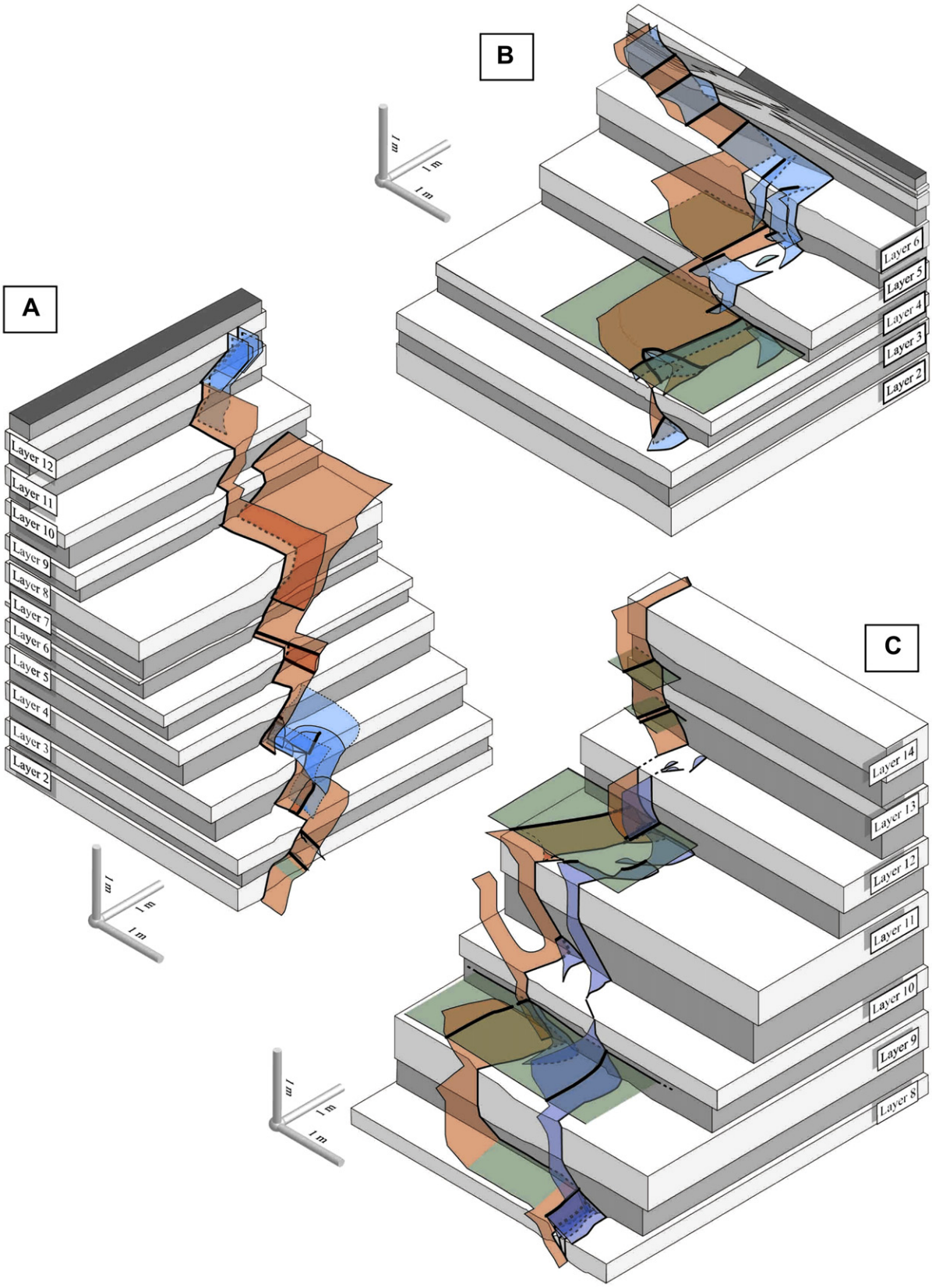

Fig. 14. 3D simplified representations of the fault shape for the three cases studied. A: Charce fault zone. B: Espreaux A fault zone. C: Espreaux B fault zone. Orange and blue are used to help visualization of fault segments. Sub-horizontal faults in clay layers are in green. Thin black continuous lines are observed traces of fault segments (dashed if behind another fault). Thick black lines are fault intersections. The very thin continuous lines are a conceptual representation of fault shape to the observed 3D evolution of fault displacement (dashed if behind another fault). They are parallel to the fault strike and dip if displacement is constant. Curved portions express decreases in displacement along the strike or the dip of the fault (tips observed when thin line joint fault trace).

increases slightly in PV. Layer 13 marks the upper fault tip and no downward decrease is observed in the lower part of the fault zone, indicating that the latter continues below the present-day erosion surface (i.e. only its upper half is now exposed). The Espreaux B fault zone displays a relatively complex displacement profile, with two displacement peaks in layer 11 and probably in layer 8 (Fig. 12B,E). The displacement profiles show significant noise along the PV profiles, with local maxima and minima. The displacement decreases rapidly to zero, in CS, between layer 11 and 12. Fault displacement is constant in layer 14 and 12. In Espreaux A (Fig. 12C,F), most of the fault zone is exposed as revealed by the continuous decrease in displacement from both sides of the displacement plateau in layers 4 and 5 where the displacement reaches a maximum 20 cm value, but the fault tips are not observed. The profile also shows significant noise in PV.

In PV, decreases along a fault segment (especially towards a tip) are in many cases more or less counterbalanced by increases along a neighbouring segment so that the cumulative displacement remains more or less constant and never falls to zero. All the fault segments therefore interact. However many complexities exist and variations in the PV cumulative displacement occur in two ways: (i) large wave changes producing global decreases or increases, (ii) second order high-frequency and local fluctuations superimposed on this large-scale tendency and introducing noise along the profile. In most cases, the latter are encountered near relay zones between fault segments as for example in Charce layer 4, Espreaux A layer 4 or Espreaux B layer 11 (Figs. 2, 4, 6 and 12). Thus these second order fluctuations are related to strike-parallel relay zones with or without linkage between the fault segments. Such displacement variations are sometimes high and greater than 30% of the cumulative displacement. The highest strike-parallel cumulative displacement gradients, greater than 0.18 and up to 0.5, are associated with these relay zones and characterize a short fault part of the fault zone length (17% of the total 1785 cm fault length). Elsewhere and thus along most of the fault zone, strike-parallel gradients are lower than 0.18. Thirty percent of the fault length has a low gradient (<0.04) and 53% has rather scattered values, averaging 0.09. Therefore, in PV, displacements on fault segments and fault zones alike exhibit similar attributes of gradient.

In clay units, the bed-normal gradient ranges are 0–0.1, 0–0.15, and 0–0.3 in Charce, Espreaux A, and Espreaux B, respectively. Fig. 13 shows that the displacement variations increase with fault length and this is independent of the fault geometry within clays (i.e. either with or without fault path along a CHF). This probably indicates that the along-dip displacement gradient is constant in clay units with a value close to 0.09. This estimation is similar to the strike-parallel gradients obtained in limestones but may be a minimum value because no reliable markers could be identified within the clay units. Notably no variation was observed in CS within limestone units and the bed-normal (and thus also along-dip) displacement gradient is therefore too low to be measured. We estimate its value to be below 0.03.

5.3. 3D displacement variations and fault zone surface

Our 3D sampling can be used to compare the strike-parallel and bed-normal displacement variations. We distinguish three types of 3D variations depending on the arrangement of the strike-parallel and bed-normal variations. In the first type, no strike-parallel variation is observed in limestone layers, whereas displacement increases or decreases through the neighbouring clays. This type occurs either near the tip area of the fault zone (for example, under layers 9 and 10 or above layer 9, Fig. 12A; above layer 12, or under layer 14, Fig. 12B), or within the fault zone (for example under layer 9, Fig. 12B; under layer 5, Fig. 12C). Such variations are likely to indicate that locally the fault surface displays horizontal elongation (i.e. aspect ratio >1). The second type of variation observed in the cumulative displacement profiles combines similar large wave strike-parallel and bed-normal variations; for example the strike-parallel decrease in Espreaux A in layer 6 and in Espreaux B in layer 9 is followed by an upward decrease. Similarly, the downward decrease in the overlying clays is followed by strike-parallel decrease at the top of Espreaux A layer 3 and Espreaux B layer 10. Such similar variations are likely to indicate that the successive PV and CS exposures move away from the local fault centre both in the strike-parallel and dip directions. For the third type, strike-parallel and bed-normal variations are locally opposite; for example, in Charce layer 3, 4 and 8, the strike-parallel decrease succeeds the bed-normal increase within the underlying clays (Fig. 12A,D). The increase in Espreaux B layer 10 succeeds the decrease in the underlying clays, whereas decreases in the overlying clays succeed small increases in the limestone layers 4 and 8 (Fig. 12B,C). These opposing variations in CS and PV may indicate that the successive PV and CS exposures moved towards the fault centre in the strike-parallel direction and away from the fault centre in the bed-normal direction. Notably, in the Charce fault zone, strike-parallel increases (layers 4, 8, 10) always occur southwards, suggesting that the exposed portion of the fault zone corresponds to its upper northern quarter. We cannot, however, exclude that these PV variations are fluctuation variations related to fault interaction, and therefore are not representative of the large-scale fault characteristics.

6. Discussion

Observations of the Charce and Espreaux exposures made it possible to establish the 3D evolution of fault characteristics of mesoscale normal fault zones that developed in multilayer sedimentary systems. The fault zones studied comprise many fault segments, which connect together to form through-going fault zones. Although the two tips of the fault zones were not systematically observed, the large vertical and lateral extents of the successive exposures allow identification and 3D correlation of most fractures of the fault zones. This study provides a basis on which to discuss fault growth processes as well as the influence of the mechanical anisotropy arising from sub-horizontal layering. A simplified 3D representation of the studied fault zones is proposed in Fig. 14.

The three normal fault zones exhibit fault refractions as a function of lithology with high dips in limestone layers and moderate or low dips in clay layers (Fig. 9). Refraction is common in multilayer sedimentary systems (Mandl, 1988; Ferrill and Morris, 2003; Schöpfer et al., 2007) and may be explained by variations in orientation or magnitude of the local effective stress state, often interplaying with the effects of friction or cohesion contrasts between adjacent layers. Several processes may cause heterogeneous stresses in multilayer systems like (1) strong coupling between layers with contrasting elastic properties preventing different layer-parallel elongations (Mandl, 1988; Bourne, 2003), (2) local fluid overpressures (Mandl, 1988), and (3) low angle simple shear in weak layers. The presence of sub-horizontal faults in clay layers (CHF) indicates that the last process may apply to the faults under study, but others necessarily operate because fault refractions also occur where such planes are absent. Marked elastic contrasts and variations in pore pressure are both likely to occur in sedimentary systems (like those consisting in alternating limestone and clay units). However, sliding on CHFs probably reflects a degree of decoupling, at least at some stage of fault development. Incidental linkage of unrelated fractures such as joints or faults initiated in limestone layers may also explain varying fault dips (Wilkins et al., 2001; Crider and Peacock, 2004). However, such

incidental linkages would necessarily imply scattering in the horizontal fault path (HPL) data; in the case under study, on the contrary, HPLs are closely correlated with the clay thickness (Fig. 11). The studied faults are thus more probably in line with the 'coherent model' of Walsh et al. (2003).

The anisotropy of the multilayer rock system not only induces variations in the attitude of fault segments but also in the fracturing mode. Fault segments exhibit little mineralization in clay layers and thick calcite in limestones, indicating opening and fluid circulation. Striations are also observed on the fault planes in the limestones, implying a sliding phase. The following scenario is speculative as it does not rely on reliable chronological data and is proposed as a basis for discussion. Following previous studies (McGrath and Davison, 1995; Peacock and Zhang, 1993; Soliva and Benedicto, 2005), we suppose that the fault zone nucleates in a more competent bed (i.e. limestones), as either hybrid or mode I fracture. The fault propagates continuously into the surrounding clays, then into the adjacent limestones, and so on. An alternative is that fractures, which should be regarded as precursor structures in the sense of Crider and Peacock (2004), occur in limestone layers first and later connect together after propagation of the fault in clays as proposed by Schöpfer et al. (2006). In the cases under study no fractures were restricted to the limestone beds, thus strengthening this second hypothesis. The deformations later proceed through a combination of pure frictional sliding and dilatational faulting. This transition may originate from a release in fluid overpressures associated with the propagation of the fault either vertically or horizontally, which induces changes in the magnitude of the local effective stress state and thus in the brittle deformation mode.

Fault growth in clay layers also includes the development of several fracture types. In addition to the $\sim 40^{\circ}$ dipping fault segments, sub-horizontal faults (CHFs) may be used to transfer normal fault displacement in clay layers. Such low angle faults are common features in weak layers of multilayer systems (Ferrill et al., 1998; Gross et al., 1997) and their occurrence is implicitly or explicitly related to other deformation processes like flexural slip folding. This is not the case in the examples studied here, because the CHFs developed under the same pre-folding tectonic phase as the main normal fault zones (see section 3.1) and no mechanism other than this extensional phase appears likely to produce bedding parallel shear in these horizontal sedimentary systems.

To our knowledge, such extension related CHFs have not been the focus of reviews in the literature. Since CHFs significantly influence fault zone geometries, we discuss the conditions under which they form below. Careful examination of the clay units indicates that the CHFs occur in both thin and thick clay units and are most frequently observed where the thickness ratio between the clays and the two adjacent limestones is low. In other words, CHFs generally nucleate in relatively thin clays overlain and underlain by relatively thick limestones, whereas they are rare in thick clay layers surrounded by thin limestones. Although some CHFs could result from local processes associated with the normal fault zone propagation, another mechanism is behind their development because some of them continue far from fault zones and others occur in clay layers not affected by the fault zones. CHFs accommodate the regional extension in clays and we suggest that they may result from stress perturbations caused by the contrasts in the elastic properties in the multilayer system. An alternative is that they reflect differential deformation modes between weak and competent layers, horizontal simple shear in the former and faulting or mode I fractures in the latter.

Displacement variations along the fault zones also show some degree of correlation with the multilayer system, suggesting that the anisotropy of the faulted rock not only influences the architecture of fault zones but also their propagation. Within clays, the along-dip gradient is close to 0.08 whatever the geometry of the fault segment (presence or absence of CHFs) whereas it is below 0.03 within the limestones. Although these values represent an average of the displacement variations within the units, such a difference in displacement gradients probably denotes that the displacement accumulation is associated with discouragement in the vertical fault propagation in the weak layers. This difference in gradients could be attributed to the contrast in Young's modulus and/or in frictional properties as well as variations in the local stress state between clays and limestones (Bürgmann et al., 1994). The flattening of the faults within clays as well as their connexions on CHFs also promotes this discouragement. Because our estimate represents minimum values due to the absence of intermediate markers within clay layers, higher gradients are not excluded in the cases under study, but without stopping fault propagation.

Displacement gradients also occur along fault strikes, at least in limestone units. Examination of these variations indicates that the 0.03 value characterizes the centre portion of fault segments whereas 0.18 to 0.7 and 0.08 values are observed near fault tips, located in the relay zone or not, respectively. The mean 0.045 Dmax/L ratio of the fault segments (two tips observed) is consistent with the 0.08 gradient when assuming a 'triangular shape' of the displacement profiles (Muraoka and Kamata, 1983; Walsh and Watterson, 1989) and therefore confirms that this gradient characterizes the horizontal propagation of the fault segments in limestones. The 0.08 gradient is close to the mean values observed along isolated faults in other carbonate units (Soliva and Benedicto, 2005). The 0.18 to 0.7 gradients are interpreted as arising from greater restriction of propagation of the fault segments when they approach the tip of a neighbouring fault (Gupta and Scholz, 2000). Interestingly, the cumulative displacement profiles display the same gradient distribution. This means that even if a fault zone comprises many segments that are genetically related and that interact, displacement analysis of the whole system may help identify the processes governing the growth of fractures. In the examples studied, preservation of the characteristic gradient values is related to the large overlap between fault segments coupled with the large flat-topped portion of the displacement profiles, as indicated by less frequent small gradients along the fault zones than along the fault segments (30% versus 60% of the total length).

Using their maximum cumulative displacements (15 cm, 20 cm and 31 cm) and the 0.08 value of the propagation gradient, the theoretical strike-parallel lengths of the Espreaux A, Espreaux B, and Charce fault zones come to 375 cm, 500 cm and 700 cm, respectively (calculated assuming a triangular shape of the displacement profiles). We observed only a portion of the faults along a horizontal distance of 510 cm, 600 cm and 675 cm and the fault zones are thus much longer than expected. These differences may reflect that the sampled section does not record the true maximal displacement. An alternative is that the faults have abnormal lengths which are consistent with the significant segmentation and the flat-topped displacement profiles of most fault segments. If true, the last fault attribute may reflect the point that the local discouragement in the vertical propagation through weak units of multilayer systems results in the horizontal growth of faults, in a similar way as for restricted faults (Nicol et al., 1996; Soliva and Benedicto, 2005). The difference between the theoretical and real length may also indicate that fault zones grow first in length and later accumulate displacement without significant enlargement, as suggested by Walsh et al. (2002). Whatever the process implicated, the 3D gradient variation, with very low values along the vertical in limestones and moderate values along the vertical and horizontal in limestones highlights the 3D complexity of fault growth in multilayer systems.

7. Conclusion

Sampling and analysis of fault characteristics in both cross-sections and plan views made it possible to characterize the 3D fracture pattern associated with three mesoscale normal faults cutting across a clay/limestone multilayer system and provided insight into the processes governing fault growth. This study ends by contributing to the assessment of fracturing characteristics in clays by the sole description of fracturing in the surrounding limestone layers. The fault zones under study are in line with a 'coherent model' but several complexities arise from the heterogeneity inherent in the multilayer system and the existence of sub-horizontal faults in clay units (CHFs):

(1) The fault zones exhibit lithologically controlled dips and segmentation variations;
(2) CHFs, which formed in response to the same tectonic event as the normal fault zones, significantly perturb the fault zone architecture;
(3) The displacement gradient varies along the fault segments and 0.08 and 0.18 to 0.7 values characterize the fault propagation and the interaction between the fault segments, respectively. Despite many segments interacting, the cumulative displacement profiles may preserve these characteristic values.
(4) The 3D distribution of gradients can be complex and several processes control fault zone growth such as discouragement in vertical propagation in clay layers and promotion of horizontal connections

Acknowledgements

This work is part of the research studies conducted by IRSN (Institut de Radioprotection et de Sûreté Nucléaire) and the UPMC (Université Pierre et Marie Curie) on fracture development in natural and heterogeneous geological systems. We thank Andy Nicol and Conrad Child for their thorough and constructive reviews and also the Associate Editor Jao Hippertt for the critiques.

References

Angelier, J., 1990. Inversion of field data in fault tectonics to obtain the regional stress. III: a new rapid direct inversion method by analytical means. Geophysical Journal International 103, 363–376.
Bergerat, F., 1987. Stress fields in the European platform at the time of Africa-Eurasia collision. Tectonics 6, 99–132.
Bott, M.H.P., 1959. The mechanics of oblique slip faulting. Geological Magazine 96, 109–117.
Bourne, S.J., 2003. Contrast of elastic properties between rock layers as a mechanism for the initiation and orientation of tensile failure under uniform remote compression. Journal of Geophysical Research 108, 2395.
Bürgmann, R., Pollard, D.D., Martel, S.J., 1994. Slip distribution on faults: effects of stress gradients, inelastic deformation, heterogeneous host-rock stiffness, and fault interaction. Journal of Structural Geology 16, 1675–1690.
Cartwright, J.A., Trudgill, B.D., Mansfield, C.S., 1995. Fault growth by segment linkage: an explanation for scatter in maximum displacement and trace length data from the Canyonlands Grabens of SE Utah. Journal of Structural Geology 17, 1319–1326.
Childs, C., Nicol, A., Walsh, J.J., Watterson, J., 1996. Growth of vertically segmented normal faults. Journal of Structural Geology 18, 1389–1397.
Crider, J.G., Peacock, D.C.P., 2004. Initiation of brittle faults in the upper crust: a review of field observations. Journal of Structural Geology 26, 691–707.
Crider, J.G., Pollard, D.D., 1998. Fault linkage: three-dimensional mechanical interaction between echelon normal faults. Journal of Geophysical Research 103, 24,372–24,391.
Ferrill, D.A., Morris, A.P., 2003. Dilational normal faults. Journal of Structural Geology 25, 183–196.
Ferrill, D.A., Morris, A.P., Jones, S.M., Stamatakos, J.A., 1998. Extensional layer-parallel shear and normal faulting. Journal of Structural Geology 20, 355–362.
Flandrin, J., 1966. Sur l'âge des principaux traits structuraux du Diois et des Baronnies. Bulletin de la Société Géologique de France 7, 376–386.
Gross, M.R., Gutiérrez-Alonso, G., Bai, T., Wacker, M.A., Collinsworth, K.B., Behl, R.J., 1997. Influence of mechanical stratigraphy and kinematics on fault scaling relations. Journal of Structural Geology 19, 171–183.
Gupta, A., Scholz, C.H., 2000. A model of normal fault interaction based on observations and theory. Journal of Structural Geology 22, 865–879.
Hancock, P.L., 1985. Brittle microtectonics: principles and practice. Journal of Structural Geology 7, 437–457.
Homberg, C., Angelier, J., Bergerat, F., Lacombe, O., 2004. Using stress deflections to identify slip events in fault systems. Earth and Planetary Science Letters 217, 409–424.
Kattenhorn, S.A., Aydin, A., Pollard, D.D., 2000. Joints at high angles to normal fault strike: an explanation using 3D numerical models of fault-perturbed stress fields. Journal of Structural Geology 22, 1–23.
Kattenhorn, S.A., Pollard, D.D., 2001. Integrating 3D seismic data, field analogs and mechanical models in the analysis of segmented normal faults in the Wytch Farm oil field, southern England. American Association of Petroleum Geologists Bulletin 85, 1183–1210.
Kim, Y.S., Peacock, D.C.P., Sanderson, D.J., 2004. Fault damage zones. Journal of Structural Geology 26, 503–517.
Kristensen, M.B., Childs, C.J., Korstgård, J.A., 2008. The 3D geometry of small-scale relay zones between normal faults in soft sediments. Journal of Strucutral Geology 30, 257–272.
Mandl, G., 1988. Mechanics of Tectonic Faulting: Model and Basic Concept. Elsevier Sci., New York.
Mansfield, C.S., Cartwright, J.A., 1996. High resolution fault displacement mapping from three-dimensional seismic data: evidence for dip linkage during fault growth. Journal of Structural Geology 18, 249–263.
Marchal, D., Guiraud, M., Rives, T., 2003. Geometric and morphologic evolution of normal fault planes and traces from 2D to 4D data. Journal of Structural Geology 25, 135–158.
McGrath, A.G., Davison, I., 1995. Damage zone geometry around fault tips. Journal of Structural Geology 17, 1011–1024.
Muraoka, H., Kamata, H., 1983. Displacement distribution along minor fault traces. Journal of Structural Geology 5, 483–485.
Nicol, A., Watterson, J., Walsh, J.J., Childs, C., 1996. The shapes, major axis orientations and displacement patterns of fault surfaces. Journal of Structural Geology 18, 235–248.
Peacock, D., Zhang, X., 1993. Field examples and numerical modelling of oversteps and bends along normal faults in cross-section. Tectonophysics 234, 147–167.
Peacock, D.C.P., Sanderson, D.J., 1991. Displacements, segment linkage and relay ramps in normal fault zones. Journal of Structural Geology 13, 721–733.
Peacock, D.C.P., Knipe, R.J., Sanderson, D.J., 2000. Glossary of normal faults. Journal of Structural Geology 22, 291–305.
Peacock, D.C.P., 2002. Propagation, interaction and linkage in normal fault systems. Earth-Science Reviews 58, 121–142.
Petit, J.P., Mattauer, M., 1995. Palaeostress superimposition deduced from mesoscale structures in limestone: the Matelles exposure, Languedoc, France. Journal of Structural Geology 17, 245–256.
Schöpfer, M.P.J., Childs, C., Walsh, J.J., 2006. Localisation of normal faults in multilayer sequences. Journal of Structural Geology 28, 816–833.
Schöpfer, M.P.J., Childs, C., Walsh, J.J., Manzocchi, T., Koyi, H.A., 2007. Geometrical analysis of the refraction and segmentation of normal faults in periodically layered sequences. Journal of Structural Geology 29, 318–335.
Segall, P., Pollard, D.D., 1980. Mechanics of discontinuous faults. Journal of Geophysical Research 85, 4350–4437.
Soliva, R., Benedicto, A., 2005. Geometry, scaling relations and spacing of vertically restricted normal faults. Journal of Structural Geology 27, 317–325.
Wallace, R.E., 1951. Geometry of shearing stress and relation to faulting. Journal of Geology 59, 118–130.
Walsh, J.J., Bailey, W.R., Childs, C., Nicol, A., Bonson, C.G., 2003. Formation of segmented normal faults: a 3D perspective. Journal of Structural Geology 25, 1251–1262.
Walsh, J.J., Nicol, A., Childs, C., 2002. An alternative model for the growth of faults. Journal of Structural Geology 24, 1669–1675.
Walsh, J.J., Watterson, J., 1989. Displacement gradients on fault surfaces. Journal of Structural Geology 11, 307–316.
Wilkins, S.J., Gross, M.R., 2002. Normal fault growth in layered rocks at Split Mountain, Utah: influence of mechanical stratigraphy on dip linkage, fault restriction and fault scaling. Journal of Structural Geology 24, 1413–1429.
Wilkins, S.J., Gross, M.R., Wacker, M., Eyal, Y., Engelder, T., 2001. Faulted joints: kinematics, displacement-length scaling relations and criteria for their identification. Journal of Structural Geology 23, 315–327.
Willemse, E.J.M., Pollard, D.D., Aydin, A., 1996. Three-dimensional analyses of slip distributions on normal fault arrays with consequences for fault scaling. Journal of Structural Geology 18, 295–309.